Supplemental Material to

"Ultrafast Demagnetization Excited by Extreme Ultraviolet Light From a Free-Electron Laser"

André Philippi-Kobs, Leonard Müller, Magnus H. Berntsen, Wojciech Roseker, Matthias Riepp, Kai Bagschik, Jochen Wagner, Robert Frömter, Miltcho Danailov, Flavio Capotondi, Emanuele Pedersoli, Michele Manfredda, Maya Kiskinova, Michal Stransky, Vladimir Lipp, Andreas Scherz, Beata Ziaja, Hans Peter Oepen, Gerhard Grübel

A) Stimulated Emission: Calculations based on modified Beer-Lambert law

We used the modified Beer-Lambert law of Ref. [1] to study the impact of stimulated emission on the scattering efficiency I_{eff}. This model simplifies the *M*-edge absorption and reduces the atomic resonance to a two-level-system (3*p*→3*d*) interacting with a coherent light field [1]. A natural decay energy width of $\Gamma = 1.64$ eV is used, corresponding to the Auger-decay time of $\tau_{\mathrm{Auger}} = \hbar/\Gamma = 0.4$ fs, see section B). For the quantitative description, the experimentally determined optical constants are used [2] to estimate the dipole-transition decay widths to 0.0113 and 0.0125 meV for the absorption of left/ right-circularly polarized light, respectively.

Within the two-level approximation the dipole-transition decay widths for the *M*-edge are about a hundred times smaller as compared to the ones found for the *L*-edge [1]. This would lead to a sizable shift of the onset of nonlinear X-ray absorption towards higher peak intensities. However, the coherent-enhancement factor $\mathcal{G}_{\mathrm{coh}} = N_a\lambda^2/(4\pi A)$, which is a measure for the coherently scattered intensity, N_a/A is the number of atoms in the beam with cross-sectional area A, is also a hundred times larger at the *M*-edges due to the larger coherence volume spanned by the longer XUV wavelength. As a result, the model predicts that the coherent response of resonant emitters, i.e., stimulated emission, occurs at the *M* and *L*-edges for intensities of the same order of magnitude.

For the calculation, the temporal FEL-pulse shape is assumed to be Gaussian with a pulse length of 70 fs (FWHM). The resulting I_{eff} vs fluence f curves are shown in Fig. S1. They follow a logistic behavior described by

$$I_{\mathrm{eff}}(f) = \left(1 + \frac{f}{\xi_{\mathrm{1P,SE}}}\right)^{-1.5}, \qquad \text{(Eq. S1)}$$

and have a characteristic $(1/e)$-fluence of $\xi_{\mathrm{1P,SE}} \approx 95$ mJ/cm² for single-pulse mode and $\xi_{\mathrm{2P,SE}} \approx 190$ mJ/cm² for double-pulse mode. The modeling shows that stimulated emission scales nonlinearly with the pulse intensity. As the two consecutive pulses in the double-pulse mode have half the peak intensity of a single pulse for the same fluence and due to the short τ_{Auger}, the double-pulse curve is shifted to twice the fluence as compared to the single-pulse

curve. Hence, stimulated emission is ruled out as predominant mechanism for the experimentally observed quenching. Notably, $\xi_{1\mathrm{P,SE}} \approx 95\ \mathrm{mJ/cm^2}$ is a factor of ≈ 3.5 larger than $\xi_{1\mathrm{P,exp}}$. Therefore, $\xi_{1\mathrm{P,SE}}$ is similar as for the *L* edges [3,4], contrary to the recent speculation in Ref. [5], which follows from the fact that differences in the respective dipole-transition decay widths are compensated by differences in the coherent-enhancement factors $\mathcal{G}_{\mathrm{coh}}$.

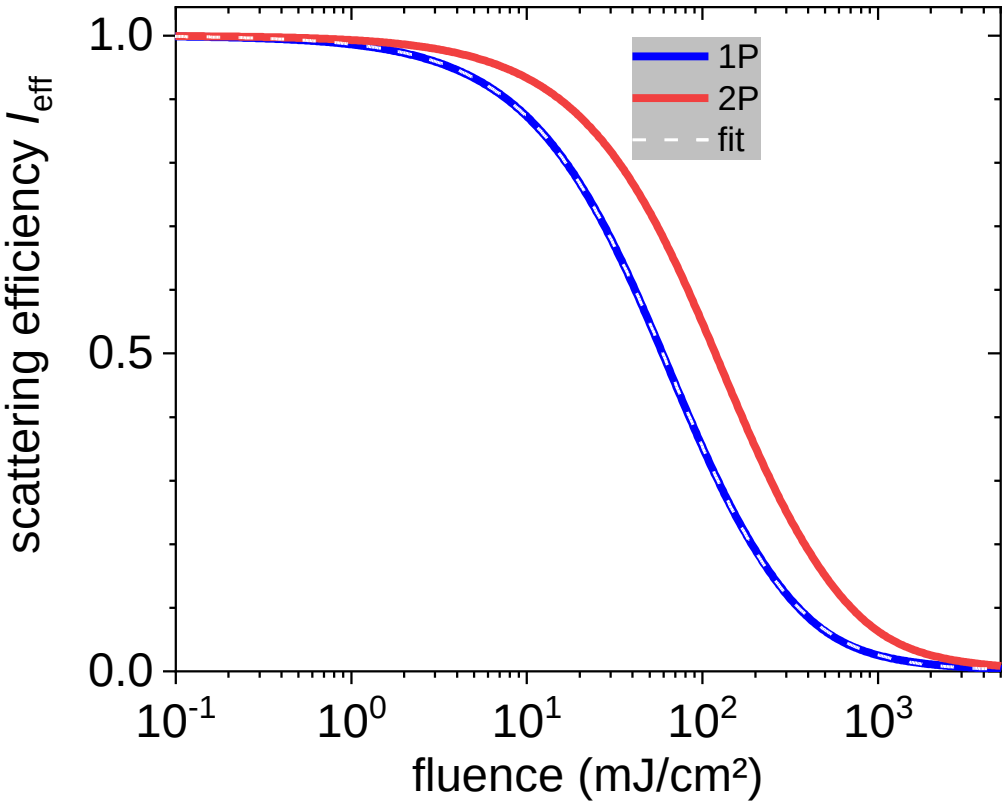

Figure S1: *Scattering efficiency vs fluence calculated by means of the modified Beer-Lambert law including stimulated emission for the single-pulse* (1P,*blue*) *and double-pulse case* (2P,*red*)*. The white dashed line overlaying the single-pulse curve is a fit to the data using Eq.* (S1)*.*

B) p-shell shift: Calculations based on kinetic Boltzmann equations

We performed calculations based on the kinetic Boltzmann equations [6-11] in atomistic approximation to model the complex transient non-equilibrium evolution of the electronic states in the Co/Pt multilayer. In particular, we estimated the average ionization degree and 3*p*-level shift as a function of fluence and time for both, single and double-pulse schemes. The calculations included the following interactions: photo and collisional ionization, three-body recombination, elastic electron–ion and electron–atom scattering and shielded electron–electron interactions. The details have been discussed in Ref. [6]. The code can simulate the evolution of irradiated atomic samples of spherical geometry assuming spatially uniform XUV intensity. Up to date, no respective fully *ab-initio* (e.g., DFT-based) calculations are feasible in solids.

We considered a multilayer sample consisting of [Co(0.8 nm)/Pt(1.4 nm)]$_7$/Co(0.8 nm) layers. The photon energy ($E = 59.6$ eV) was set slightly above the cobalt 3*p*-3*d* resonance. Cross sections and rates for photo-induced processes were estimated using the XATOM code [12]. Charge-screening-induced shifts of atomic orbitals were calculated with the Debye model, applicable in the ionization regime, considered here. Collisional cross-sections were estimated from the Lotz formula [13]. The simulations were performed for temporal Gaussian pulse profiles with a pulse length of 70 fs (FWHM) and a peak-to-peak separation of 250 fs in case of double-pulse mode, varying the fluence between 0.21 and 140 mJ/cm² (Fig. S3(a)). The simulations were terminated 140 fs after the peak of the (second) pulse. Here, we restrict ourselves to show the results for Co only; the results for Pt ionization are similar, however, with the degree of ionization at a given fluence slightly reduced as compared to the one of Co, see also (Supplemental Materials to) Ref. [14].

Fig. S2(b) shows the ionization as a function of time before, during, and after the impact of the pulse(s) (same time scale as in Fig. S2(a)).After the impact of the pulses, the final ionization degree is the same for both pulse schemes when the same integral fluence is used. Fig. S2(c) depicts the final average ionization degree of Co as a function of fluence 150 fs after the impact of a single and double pulse. The calculations further show that the Auger process with a characteristic time of $\tau_{\mathrm{Auger}} = 0.4$ fs dominates the decay of the initial 3*p*-3*d* excitation. Thereby, the dominant process is the repopulation of the 3*p*-state via a 3*p*-3*d* transition and the generation of a hot electron from the 3*d* level with energies of up to 60 eV. Again, the ionization state is the same for both, single and double pulses, as the intra-pulse ionization (after τ_{Auger}) proceeds quasi-instantaneously on a sub-femtosecond timescale after each photon impact, and as recombination processes are rare (Fig. S2(b)). The subsequent long-timescale interactions of the hot electrons with phonons and magnons are not considered in the model. The presence of excited electrons only slightly affects the energy difference

between the 3*p* and 3*d*-states, i.e., E_{3p-3d}, as can be seen in Fig. S2(d) where E_{3p-3d} vs fluence and ionization is given at 500 fs. The curves show a rather flat behavior revealing that the position of energy levels is dictated by the ionization state. For Co^{1+} (Co^{2+}) the energy shift is about 0.8 eV (1.4 eV), so that Co^{2+} fairly meets the resonance condition used in the experiment. By using the scattering intensity I vs photon energy E_{ph} curve (Fig. 1(b) in the main text), the fraction of ionization N_i vs fluence f (Fig. S2(c); N_0: uncharged state), and the level shift ΔE_i for different ionization states (Fig. S2(d), thereby neglecting the small fluence dependence of ΔE_i), the fluence dependence of the scattering efficiency is estimated as

$$I_{\mathrm{eff}}(f) = \sum_{i=0}^{2} I\left(E_{\mathrm{ph}} + \Delta E_i(f=0)\right) N_i(f)/(I(E_{\mathrm{ph}})N_0), \qquad \text{Eq. (S2)}$$

considering ionization states up to Co^{2+} ($i = 2$) for $E_{\mathrm{ph}} = E_{\mathrm{res}}$ and $E_{\mathrm{ph}} = E_{\mathrm{res}} + 1.5$ eV, see Fig. S2(e).

To sum up, Fig. S2(e) shows $I_{\mathrm{eff}}(f)$ deduced from calculations including a *p*-shell-shift induced by a charged environment of excited electrons that results from the initial 3*p*-3*d* transitions and subsequent Auger decays. No difference in $I_{\mathrm{eff}}(f)$ between the single and double-pulse calculations is obtained. For the detuned case that mimics the experiment, $I_{\mathrm{eff}}(f)$ initially increases as the resonance condition of the 3*p*-3*d* transition shifts to higher energies. Eventually, $I_{\mathrm{eff}}(f)$ would decrease with further increasing fluence (not shown). The absence of an initial increase in the experimental $I_{\mathrm{eff}}(f)$ data reveals that the *p*-level shift cannot explain the observed quenching. For the resonant case, a characteristic quenching fluence of $\xi_{\mathrm{level-shift}} \approx 550\ \mathrm{mJ/cm^2}$ is estimated. This order of magnitude (J/cm² regime) is in accordance with studies on metallic systems dealing with XUV-induced changes of optical parameters [15,16,17], and shifting of bands or absorption edges [18-20].

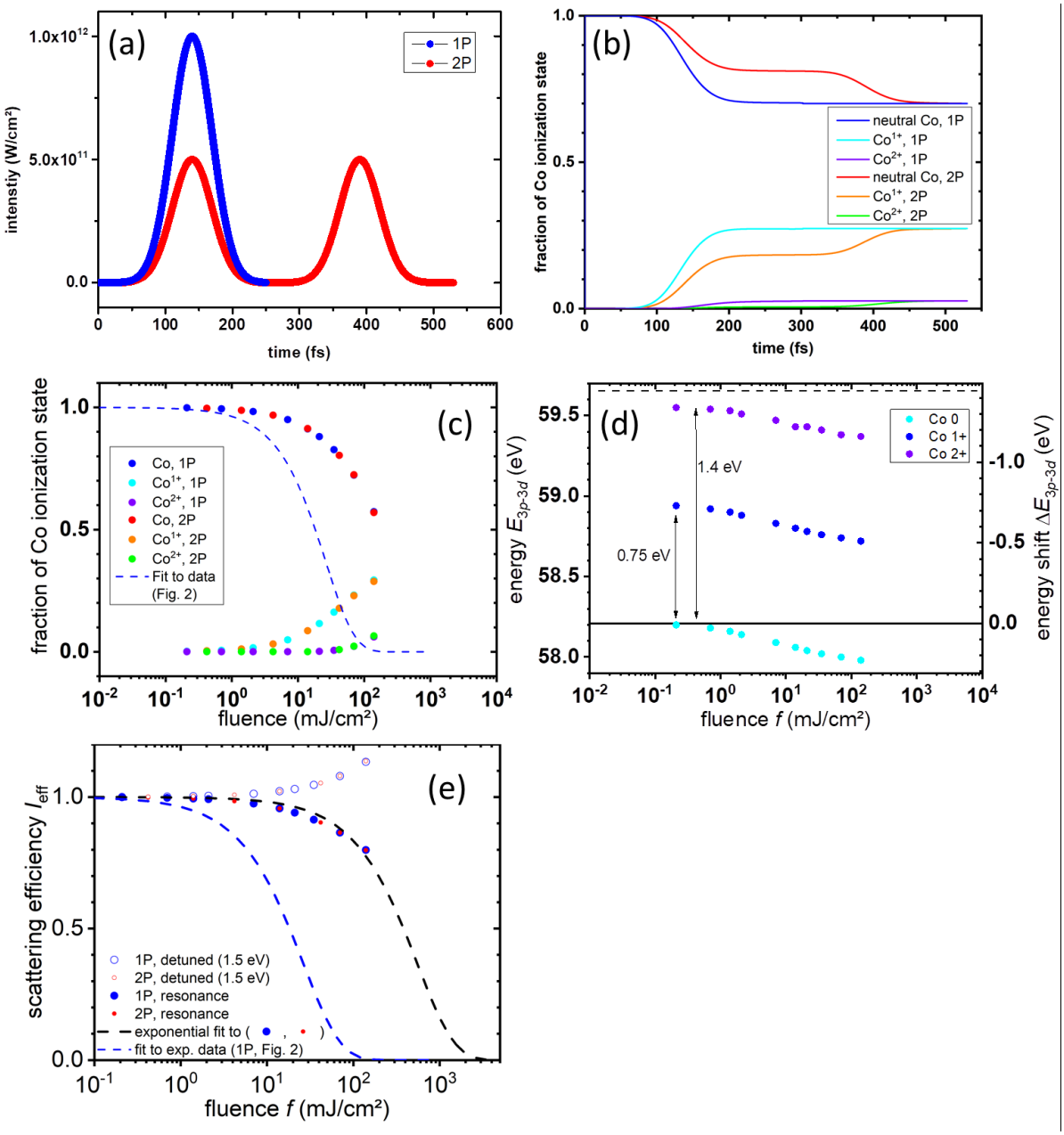

Figure S2: *Results of the kinetic Boltzmann calculations.* (*a*) *Temporal pulse profiles and* (*b*) *transient fraction of Co ions for single* (1P) *and double-pulses* (2P) *with a* (*combined*) *fluence of* $f = 70$ mJ/cm². (*c*) *Final fractions of Co ions* N_i (*at* 500 fs) *as a function of fluence* f *and (d) energy difference* $E_{3p-3d}(f)$ *and level shift* $\Delta E(f, N_i) = E_{3d-3p}(f, N_i) - E_{3d-3p}(f = 0, N_i)$. *The dashed line in* (*d*) *shows the experimentally used shift away from the* $3d - 3p$ *resonance.* (*e*) *Calculated scattering efficiency vs fluence curves for detuned* (*by 1.5* eV above resonance) *and resonant conditions, i.e., Fig. 3*(*g*) *given in the main text.*

C) Phenomenological model of intra-pulse demagnetization

For the pulses of the single and double-pulse modes, a Gaussian time profile with a FWHM of $t_{\mathrm{FEL}} = 70$ fs is considered (Fig. S3). For the double-pulse mode, the peak intensities of the sub-pulses are delayed by 200 fs. Further, a linear relation between degree of demagnetization and pulse fluence (time-integrated intensity) is assumed, i.e., the normalized saturation magnetization M_{S} decreases with normalized fluence c according to

$$M_{\mathrm{S}}(c) = 1 - c, \qquad \text{Eq. (S3)}$$

as it is frequently found experimentally even for high demagnetization strengths of up to 90% [21,22]. The scaling of fluence is done such that a single or double-pulse with a fluence of $c = 1$ fully demagnetizes the sample for $t \to \infty$ omitting remagnetization since electron-phonon thermalization or heat dissipation act on longer time scales of a few and hundreds of picoseconds, respectively. This implies that the sub-pulses in the double-pulse mode have only half the (peak) intensity as compared to the single pulse for the same fluence value. For $c > 1$ already a part of the pulse leads to complete demagnetization. Note that, depending on fluence c and/or demagnetization time τ_{demag}, the magnetization reaches zero before the end of the pulse.

The calculations are performed for fluences in the range of $0.01 < c < 100$. Time steps of $\Delta t \approx 0.2$ fs are used ($n = 5000$ equidistant steps in the time range of $t_{\mathrm{min}} = -400$ fs to $t_{\mathrm{max}} = +500$ fs and $t_{\mathrm{min}} = -500$ fs to $t_{\mathrm{max}} = +600$ fs for the single-pulse and double-pulse scenario, respectively; $t = 0$ corresponds to the center of the pulse pattern), i.e., much smaller than the demagnetization time of $\tau_{\mathrm{demag}} \approx 7$ fs determined from the experimental data (see below). For each time step $t' = t_{\mathrm{min}} + k\Delta t,\ k = 1 \ldots n$, the photo-induced demagnetization process is initiated and proceeds for $t > t'$ with a characteristic demagnetization time τ_{demag} leading to a relative reduction of M_{S} (Fig. S4) according to

$$\delta M_{\mathrm{S},k}(t) = c \cdot \tilde{\imath}_k \left(1 - \exp\left(-\frac{t-(t_{\mathrm{min}}+k\Delta t)}{\tau_{\mathrm{demag}}}\right)\right). \qquad \text{Eq. (S4)}$$

$\tilde{I}_k = c \cdot \tilde{\imath}_k$ is the partial fluence in a given time interval with $\tilde{\imath}_k = \int_{t'-\Delta t}^{t'} i(t)\,\mathrm{d}t$, where $i(t)$ is the Gaussian function with an integral value of 1. The transient saturation magnetization (normalized to 1) is then given by the summation of the demagnetization of all time slices according to:

$$M_{\mathrm{S}}(t) = 1 - \sum_{k=1}^{n} \delta M_{\mathrm{S},k}(t). \qquad \text{Eq. (S5)}$$

For $c > 1$ mathematically obtained negative M_{S} values are set to zero for the remaining time steps for the subsequent calculations. The resulting unphysical discontinuity in $\mathrm{d}M_{\mathrm{S}}/\mathrm{d}t$ at $M_{\mathrm{S}} = 0$ (Fig. S5) is connected with the assumption of a linear relation between demagnetization and fluence but does not provide a relevant error in the modeling of the scattering efficiency as

outlined in footnote Ref. [23]. The transient magnetic scattering is proportional to $I_f(t') = (M_S(t'))^2 \cdot \tilde{I}_k$ (Fig. S5). For intense pulses ($c \gg 1$) the sample scatters only in the beginning of the pulse, depending on values of c and τ_{demag}.

For a fixed fluence c, summing up $I_f(t')$ over the whole duration of the pulse or double pulse, respectively, yields the total scattering intensity $S(c) = \sum_{t'} I_f(t')$. Dividing $S(c)$ by the incident number of photons $N_{\mathrm{ph}} \propto c$ and normalizing it to the respective low fluence values for $c = 0.01$ finally provides the scattering efficiency vs fluence behavior (Fig. S6)

$$I_{\mathrm{eff}}(c) = (S(c)/c)/(S(c = 0.01)/0.01). \qquad \text{Eq. (S6)}$$

Note particularly that the total scattered intensity S rises linearly for low fluences of $c \ll 1$ (Fig. S6). For higher fluences, the $S(c)$ curve flattens out. The transition region and its width in fluence depend on the set demagnetization time. Generally, the transition happens when parts of the single or double pulses do not scatter anymore, due to complete demagnetization. For a quasi-instantaneous demagnetization, $\tau_{\mathrm{demag}} = 1$ fs, this is the case (for both pulse schemes) as soon as a fluence of $c = 1$ is reached. Consequently, the transition from linear increasing to almost constant scattering intensity vs fluence behavior occurs in the vicinity of $c = 1$. For the longest demagnetization time $\tau_{\mathrm{demag}} = 200$ fs, in contrast, the pulse scheme plays a role. For $c = 2$, the magnetization reaches zero at the end of the second sub-pulse (Fig. S5(b)), whereas for the single pulse (Fig. S5(a)), a fluence of $c = 3$ is needed to completely demagnetize the sample before the pulse ends. This explains the flattening of the single-pulse $S(c)$ curve and the initial flattening of the double pulse $S(c)$ curve (Fig. S6). At higher fluences, the latter curve converges with the single-pulse curve and, as a consequence, has a kink in the fluence range $c \approx 3 \ldots 6$. At $c = 6$ the first pulse leads to $M_S = 0$ before the second pulse starts and hence at this fluence the crossover to the single-pulse behavior is completed.

The simultaneous fitting of the $I_{\mathrm{eff}}(c)$ model curves for single and double pulses to the respective $I_{\mathrm{eff}}(f)$ experimental curves allows for determining the demagnetization time τ_{demag} and the fluence for complete demagnetization f_{demag} ($\widehat{=}\ c = 1 : M_S(t \to \infty) = 0$). As a result, a demagnetization time of $\tau_{\mathrm{demag}} = (7 \pm^{12}_{7})$ fs and a demagnetization fluence of $f_{\mathrm{demag}} = (23 \pm 5)$ mJ/cm² is obtained. In particular, the corresponding model curves fairly reproduce the difference in characteristic fluence $\frac{\xi_{1\mathrm{P,exp}}}{\xi_{2\mathrm{P,exp}}} \approx 1.05$ found experimentally (given in the main text). For the fitting, a relative systematic error in the fluence determination between both pulse modes of $\pm 5\%$ was considered, which is related to slightly different beam sizes resulting from different source points for the FEL radiation between both operation modes [24]. Importantly,

for a proper deduction of the *effective* f_{demag} the two-dimensional Gaussian-beam profile has to be considered as outlined in the following section D.

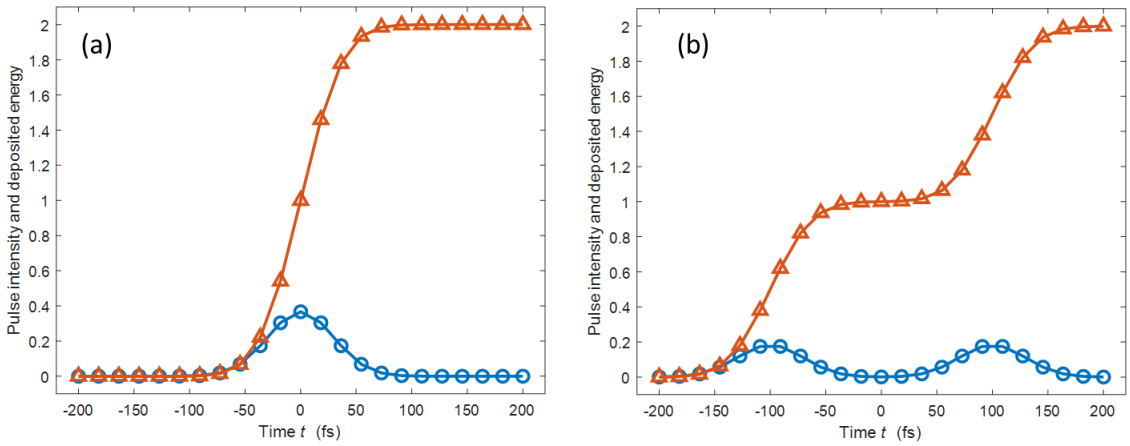

Figure S3: *Temporal pulse profile* (*blue*) *and integrated photon flux/ deposited energy* (*red*) *for* (*a*) *single and* (*b*) *double-pulse mode. As the pulse shape is assumed to be Gaussian, the deposited energy rises like a single or double error function, respectively. For both figures, the total number of photons equals to a fluence of* $c = 2$*, i.e., full demagnetization is achieved by half of the single, or the first of the double pulses. For illustration purposes, only* $n = 23$ *time slices are used instead of* $n = 5000$ *used for the calculations.*

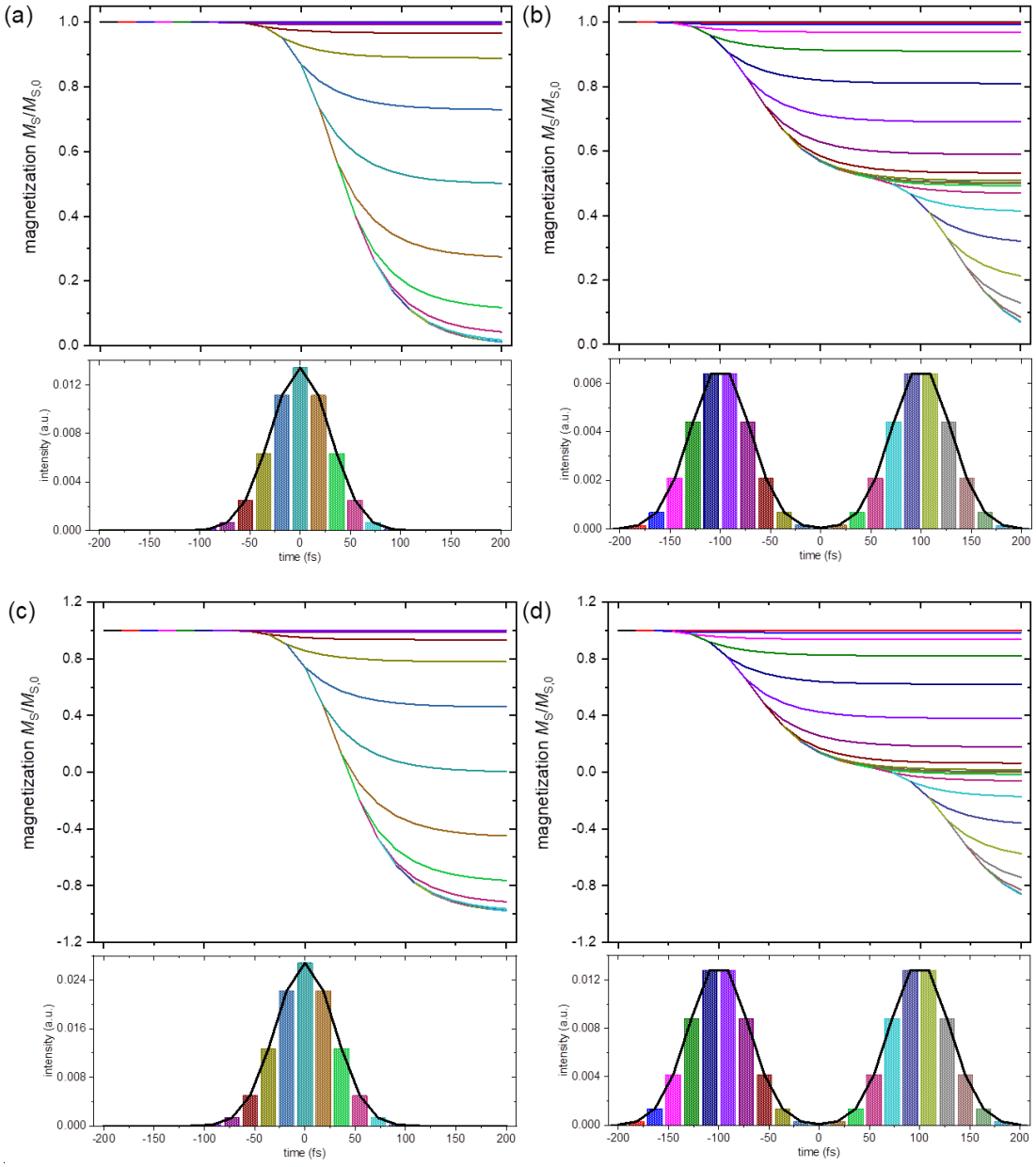

Figure S4: *Impact of individual discretized pulse slices on the evolution of the magnetization for* (*a*),(*c*) *single and* (*b*),(*d*) *double pulses and a demagnetization time of* $\tau_{\mathrm{demag}} = 40$ fs*. For* (*a*),(*b*) *and* (*c*),(*d*) *the integral fluence is* $c = 1$ *and* $c = 2$*, respectively. Note that unphysical* $M_S < 0$ *values are set to* $M_S = 0$ *for the remaining time steps in the subsequent calculations. For illustration, only* $n = 23$ *slices are used instead of* $n = 5000$ *used for the calculations.*

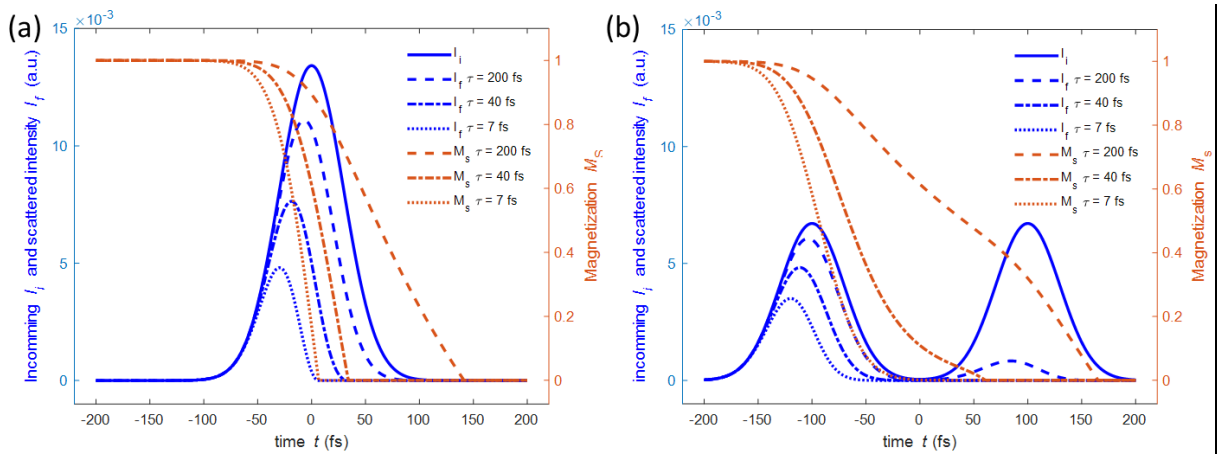

Figure S5: *Time-dependent saturation magnetization* $M_S(t)$ (*brown curves, negative values are set to zero*) *and scattering intensity* $I_f(t)$ (*dashed blue curves*) *for a pulse intensity of* $c = 2$ *and a demagnetization time of* τ_{demag} =200 fs (*elemental* Co), 40 fs (Co/Pt *multilayers*), *and* 7 fs *describing the result of the experimental study. Note that for both,* (a) *single and* (*b*) *double-pulse mode the total scattered intensity is strongly decreased with decreasing demagnetization time. In addition, already for* $\tau_{\mathrm{demag}} = 40$ fs, *the second pulse only scatters weakly as the magnetization has almost vanished already at the beginning of the second pulse. For clarity, both figures are plotted on the same scale.*

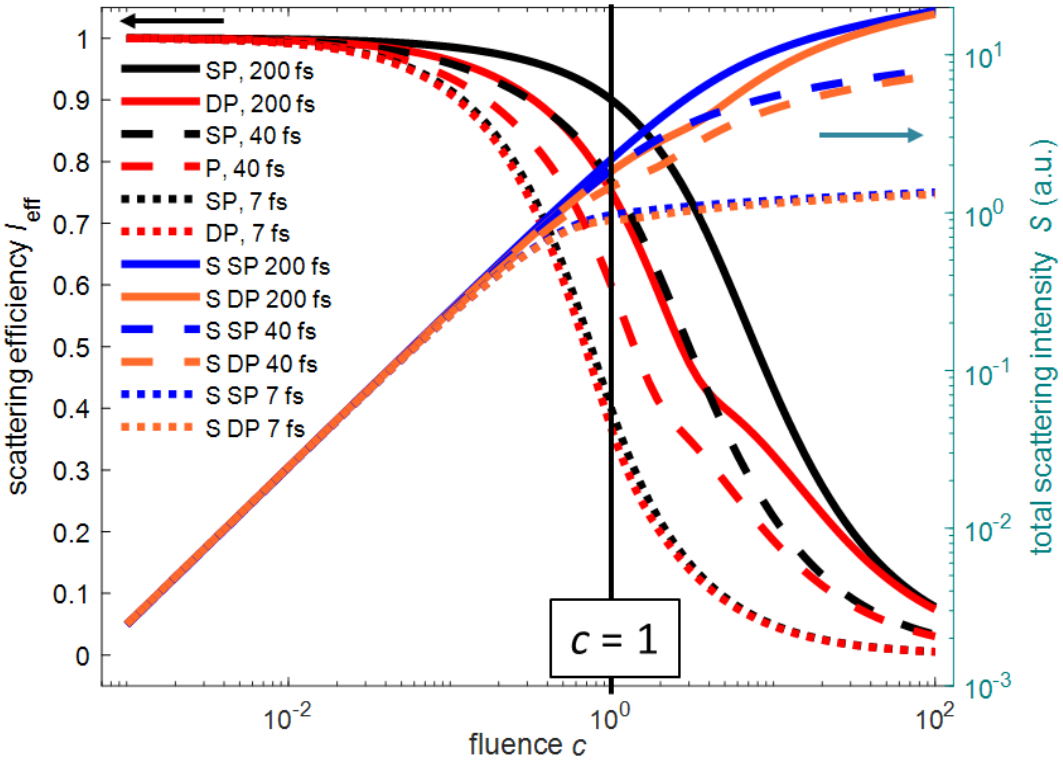

Figure S6: *Scattering efficiency* I_{eff} *and total scattering intensity* S *as a function of fluence* c *for demagnetization times of* $\tau_{\mathrm{demag}} = 200$ fs (*elemental* Co), 40 fs (Co/Pt *multilayers*), *and* 7 fs (*this study*). *For* $\tau_{\mathrm{demag}} = 200$ fs *and* 40 fs, *the double-pulse* $I_{\mathrm{eff}}(c)$ *curve lies significantly below the single-pulse* $I_{\mathrm{eff}}(c)$ *curve. The solid line at* $c = 1$ *indicates the minimum fluence for complete demagnetization.*

D) Impact of Two-Dimensional Gaussian-Beam Profile on Demagnetization

The lateral 2D-Gaussian beam profile has a significant influence on the definition of the fluence leading to complete demagnetization and to the fluence scale in general as outlined in the following. Normally, pump-probe experiments are performed such that the pump pulse is significantly larger than the probe pulse, so that a homogeneously pumped area (irradiated with a certain peak fluence c) is probed. Here, in the present experiment, the XUV pulse(s) acts simultaneously as pump and probe and the shape is 2D-Gaussian, see section III.
We calculated the impact of a 2D Gaussian-pulse profile on the detected overall scattering efficiency. When assuming a linear relation between demagnetization strength and fluence c, for a beam-intensity profile

$$I(x,y,c) = ce^{-x^2-y^2} \quad \text{(Eq. S7)}$$

the normalized magnetization M_S along the x and y-directions is given by

$$M_S(x,y,c) = 1 - ce^{-x^2-y^2}. \quad \text{(Eq. S8)}$$

The scattered intensity normalized to the number of incoming photons is

$$I_{\text{eff,Gaussian}}(c) = \frac{\iint_{-\infty}^{\infty} M_S^2(x,y,c)\cdot I(x,y,c)\,\mathrm{d}x\mathrm{d}y}{\iint_{-\infty}^{\infty} I(x,y,c)\,\mathrm{d}x\mathrm{d}y} = \begin{cases} \frac{1}{3}c^2 - c + 1 & \text{for } c \le 1 \\ \frac{1}{3c} & \text{for } c > 1 \end{cases}, \quad \text{(Eq. S9)}$$

when setting negative M_S-values to zero. (This expression already corresponds to the scattering efficiency since $\lim_{c\to 0} I_{\text{eff,Gaussian}}(c) = 1$ and is independent of the beam size). In this case, $c = 1$ corresponds to the fluence for which the sample gets completely demagnetized within the center of the beam. In contrast, for a homogeneously pumped sample with magnetization $M_S(x,y,c) = 1 - c$ (classical pump-probe experiment), we simply obtain (again independent of the beam size)

$$I_{\text{eff,homog.}}(c) = \frac{\iint_{-\infty}^{\infty}(1-c)^2\cdot I(x,y,c)\,\mathrm{d}x\mathrm{d}y}{\iint_{-\infty}^{\infty} I(x,y,c)\,\mathrm{d}x\mathrm{d}y} = \frac{(1-c)^2\iint_{-\infty}^{\infty} I(x,y,c)\,\mathrm{d}x\mathrm{d}y}{\iint_{-\infty}^{\infty} I(x,y,c)\,\mathrm{d}x\mathrm{d}y} = (1-c)^2 = M_S^2(\mathrm{x},\mathrm{y},\mathrm{c}). \quad \text{(Eq. S10)}$$

Both curves, $I_{\text{eff,Gaussian}}(c)$ and $I_{\text{eff,homog.}}(c)$ are shown in Fig. S7. Obviously, they are similar at low fluences but $I_{\text{eff,Gaussian}}(c)$ is shifted to higher fluences. This is reasonable, since, for instance, for a complete demagnetization in the center of the Gaussian beam, a magnetization in the flanks remains providing a magnetic scattering signal. Importantly, although we have a laterally inhomogeneous pumping (and probing) in our experiment, a rescaling of the fluence scale by $c \to 2c$ for $I_{\text{eff,Gaussian}}(c)$ approximately provides a congruent behavior of $I_{\text{eff,Gaussian}}(2c)$ and $I_{\text{eff,homog.}}(c)$ for all scattering efficiencies experimentally obtained ($I_{\text{eff}} \gtrapprox 0.2$, Fig. 2), see Fig. S8(b). Since $I_{\text{eff,Gaussian}}(c)$ can be mapped to the standard $I_{\text{eff,homog.}}(c)$

behavior of a classical pump-probe experiment (and since the mapping is particularly valid for every time slice in (the modeling of) the intra-pulse demagnetization) a comparison of, e.g., the demagnetization fluence $c = 1 \mathrel{\widehat{=}} f_{\mathrm{demag}}$ with the outcome of classical pump-probe experiments is possible. The rescaling of the demagnetization fluence $f_{\mathrm{demag,Gaussian}} = (23 \pm 5)$ mJ/cm² determined from the experimental data with the help of the phenomenological model for intra-pulse demagnetization (section C) leads to $f_{\mathrm{demag,homog.}} = 0.5 \cdot (23 \pm 5)$ mJ/cm² $= (12 \pm 3)$ mJ/cm². This value is compared in the main text with the demagnetization fluence estimated for a nominal identical Co/Pt multilayer in a conventional pump-probe experiment using NIR light.

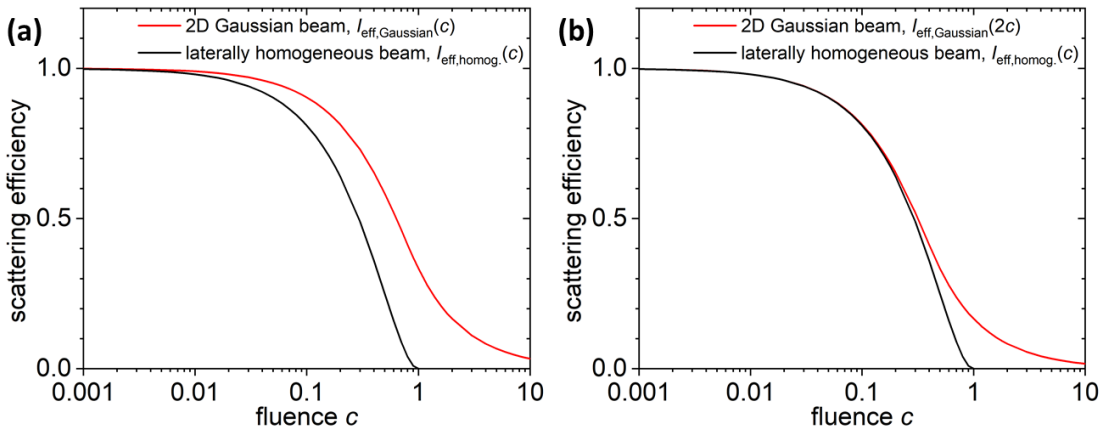

Fig. S7: (*a*) *Scattering efficiency vs fluence behavior for a 2D Gaussian-beam profile,* $I_{\mathrm{eff,Gaussian}}(c)$ (*red*)*, and a laterally homogeneous pump pulse,* $I_{\mathrm{eff,homog.}}(c)$ (*black*). (*b*) *displays* $I_{\mathrm{eff,Gaussian}}(2c)$ (*red*) *and* $I_{\mathrm{eff,homog.}}(c)$ (*black*).

E) Inelastic Mean-free Path

The electron-electron scattering time $\tau_{e^-e^-}$ is estimated from [25]

$$\lambda(E) = a_{111}\left(\frac{538}{E^2} + 0.41\sqrt{a_{111}E}\right), [E] = \text{eV}, [a_{111}] = [\lambda] = \text{nm} \quad \text{(Eq. S11)}$$

via

$$\tau_{e^-e^-}(E) = \frac{\lambda(E)}{v} \approx \frac{\lambda(E)}{6\sqrt{E}}, [E] = \text{eV}, [\lambda] = \text{Å}, [\tau_{e-e}] = \text{fs} \quad \text{(Eq. S12)}$$

thereby using the classical limit for the kinetic energy, $E = m_e v^2/2$ (m_e: electron mass), and the Co-interlayer distance of $a_{[111]} = (0.2193 \pm 0.005)$ nm determined for the fcc(111) out-of-plane textured multilayer [26]. The value for $\lambda(60\ \text{eV}) = 0.36\ \text{nm}$ is in good agreement with the NIST Database ($\lambda_{Co}(60\ \text{eV}) = 0.39\ \text{nm}$) [27].

References

[1] J. Stöhr and A. Scherz, Phys. Rev. Lett. **115**, 107402 (2015).

[2] S. Valencia, A. Gaupp, W. Gudat, H.-Ch. Mertins, P. M. Oppeneer, D. Abramsohn, C. M. Schneider, N. J. Phys. **8**, 254 (2006).

[3] B. Wu, T. Wang, C. E. Graves, D. Zhu, W. F. Schlotter, J. J. Turner, O. Hellwig, Z. Chen, H. A. Dürr, A. Scherz, J. Stöhr, Phys. Rev. Lett. **117**, 027401 (2016).

[4] J. Stöhr and A. Scherz, Phys. Rev. Lett. **115**, 107402 (2015).

[5] M. Schneider, B. Pfau, C. M. Günther, C. von Korff Schmising, D. Weder, J. Geilhufe, J. Perron, F. Capotondi, E. Pedersoli, M. Manfredda, M. Hennecke, B. Vodungbo, J. Lüning, S. Eisebitt, Phys. Rev. Lett. **125**, 127201 (2020).

[6] B. Ziaja et al., EPJD **40**, 465 (2006).

[7] B. Ziaja, H. Wabnitz, E. Weckert, and T. Moeller, New J. Phys. **10**, 043003 (2008).

[8] B. Ziaja, H. Wabnitz, E. Weckert, and T. Moeller, Euro. Phys. Lett. **82**, 24002 (2008).

[9] F. Wang, E. Weckert, and B. Ziaja, J. Plasma Phys. **75**, 289 (2009).

[10] B. Ziaja, T. Laarmann, H. Wabnitz, F. Wang, E. Weckert, C. Bostedt, T. Moeller, New J. Phys **11**, 103012 (2009).

[11] B. Ziaja, H. Wabnitz, F. Wang, E. Weckert, T. Moeller, Phys. Rev. Lett. **102**, 205002 (2009).

[12] S.-K. Son, L. Young, R. Santra, Phys. Rev. A **83**, 033402 (2011).

[13] H.-K. Chung, M. Chen, W. Morgan, Y. Ralchenko, R. Lee, H. Ener. Dens. Phys. **1**, 3 (2005).

[14] L. Müller, C. Gutt, B. Pfau, S. Schaffert, J. Geilhufe, F. Büttner, J. Mohanty, S. Flewett, R. Treusch, S. Düsterer, H. Redlin, A. Al-Shemmary, M. Hille, A. Kobs, R. Frömter, H. P. Oepen, B. Ziaja, N. Medvedev, S.-K. Son, R. Thiele, R. Santra, B. Vodungbo, J. Lüning, S. Eisebitt, G. Grübel, Phys. Rev. Lett. **110**, 234801 (2013).

[15] B. Nagler, U. Zastrau, R. R. Fäustlin, S. M. Vinko, T. Whitcher, a. J. Nelson, R. Sobierajski, J. Krzywinski, J. Chalupsky, E. Abreu, S. Bajt, T. Bornath, T. Burian, H. Chapman, J. Cihelka, T. Döppner, S. Düsterer, T. Dzelzainis, M. Fajardo, E. Förster, C. Fortmann, E. Galtier, S. H. Glenzer, S. Göde, G. Gregori, V. Hajkova, P. Heimann, L. Juha, M. Jurek, F. Y. Khattak, A. R. Khorsand, D. Klinger, M. Kozlova, T. Laarmann, H. J. Lee, R. W. Lee, K.-H. Meiwes-Broer, P. Mercere, W. J. Murphy, A. Przystawik, R. Redmer, H. Reinholz, D. Riley, G. Röpke, F. Rosmej, K. Saksl, R. Schott, R. Thiele, J. Tiggesbäumker, S. Toleikis, T. Tschentscher, I. Uschmann, H. J. Vollmer, J. S. Wark, Nat. Phys. **5**, 693 (2009).

[16] A. Di Cicco, K. Hatada, E. Giangrisostomi, R. Gunnella, F. Bencivenga, E. Principi, C. Masciovecchio, A. Filipponi, Phys. Rev. B **90**, 220303(R) (2014).

[17] E. Principi, E. Giangrisostomi, R. Cucini, F. Bencivenga, A. Battistoni, A. Gessini, R. Mincigrucci, M. Saito, S. Di Fonzo, F. D'Amico, A. Di Cicco, R. Gunnella, A. Filipponi, A. Giglia, S. Nannarone, C. Masciovecchio, Struct. Dyn. **3**, 023604 (2016).

[18] S. M. Vinko, U. Zastrau, S. Mazevet, J. Andreasson, S. Bajt, T. Burian, J. Chalupsky, H. N. Chapman, J. Cihelka, D. Doria, T. Döppner, S. Düsterer, T. Dzelzainis, R. R. Fäustlin, C. Fortmann, E. Förster, E. Galtier, S. H. Glenzer, S. Göde, G. Gregori, J. Hajdu, V. Hajkova, P. A. Heimann, R. Irsig, L. Juha, M. Jurek, J. Krzywinski, T. Laarmann, H. J. Lee, R.W. Lee, B. Li, K.-H. Meiwes-Broer, J. P. Mithen, B. Nagler, A. J. Nelson, A. Przystawik, R. Redmer, D. Riley, F. Rosmej, R. Sobierajski, F. Tavella, R. Thiele, J. Tiggesbäumker, S. Toleikis, T.

Tschentscher, L. Vysin, T. J. Whitcher, S. White, J. S. Wark, Phys. Rev. Lett **104**, 225001 (2010).

[19] B. I. Cho, K. Engelhorn, A. A. Correa, T. Ogitsu, C. P. Weber, H. J. Lee, J. Feng, P. A. Ni,Y. Ping, A. J. Nelson, D. Prendergast, R.W. Lee, R.W. Falcone, P. A. Heimann, Phys. Rev. Lett. **106**, 167601 (2011).

[20] E. Bévillon, J. P. Colombier, V. Recoules, R. Stoian, Phys. Rev. B **89**, 115117 (2014).

[21] T. Roth, A. J. Schellekens, S. Alebrand, O. Schmitt, D. Steil, B. Koopmans, M. Cinchetti, M. Aeschlimann, Phys. Rev. X **2**, 021006 (2012).

[22] N. Bergeard, M. Hehn, S. Mangin, G. Lengaigne, F. Montaigne, M. L. M. Lalieu, B. Koopmans, G. Malinowski, Phys. Rev. Lett. **117**, 147203 (2016).

[23] A linear relation between demagnetization and fluence is generally found, which is fulfilled for demagnetization strengths of up to 0.9, see e.g., Ref. [12]. However, for high fluences a violation of the linear relation is often reported. For instance, a saturation of demagnetization was observed for a Ni film by Bergeard et al., Ref. [13], that already sets in for demagnetization strengths of $\gtrapprox 0.7$ (residual magnetization of $M_S \lessapprox 0.3$). Considering such a saturation of demagnetization would eliminate the discontinuity in $\mathrm{d}M_S/\mathrm{d}t$ at $M_S(t) = 0$ for all fluences $c > 1$. If we would further assume a similar saturation of demagnetization as Bergeard et al., the maximum error of using the discontinuity (i.e., using a linear demagnetization vs fluence behavior up to $c = 1$,) on the scattering efficiency $I_{\mathrm{eff}} \propto M_S^2$ is much smaller than $0.3^2 \approx 0.1$ even for high fluences and can therefore be neglected in a good approximation. To stress the point, the scattering technique $\left(I_{\mathrm{eff}} \propto M_S^2\right)$ is very sensitive to detect small and moderate changes in M_S when it is close to the unpumped M_S but rather insensitive to changes when M_S gets close to zero, so that we cannot draw any conclusion about the demagnetization vs fluence behavior at high fluences from the modeling of the experimental data.

[24] E. Allaria, F. Bencivenga, R. Borghes, F. Capotondi, D. Castronovo, P. Charalambous, P. Cinquegrana,M.B. Danailov, G. De Ninno, A. Demidovich, S. Di Mitri, B. Diviacco, D. Fausti, W.M. Fawley, E. Ferrari, L. Froehlich, D. Gauthier, A. Gessini, L. Giannessi, R. Ivanov, M. Kiskinova, G. Kurdi, B. Mahieu, N. Mahne, I. Nikolov, C. Masciovecchio, E. Pedersoli, G. Penco, L. Raimondi, C. Serpico, P. Sigalotti, S. Spampinati, C. Spezzani, C. Svetina, M. Trovò, M. Zangrando, Nat. Commun. **4**, 2476 (2013).

[25] M. P. Seah, W. A. Dench, Surf. Interface Anal. **1**, 1 (1979).

[26] G. Winkler, A. Kobs, A. Chuvilin, D. Lott, A. Schreyer, H. P. Oepen, J. Appl. Phys. **117**, 105306 (2015), A. Kobs, Ph.D. thesis, Universität Hamburg, 2013.

[27] C. J. Powell and A. Jablonski, NIST Electron Inelastic-Mean-Free-Path Database, Version 1.2, SRD 71, National Institute of Standards and Technology, Gaithersburg, MD (2010).